Article

Abnormal beam steering with kirigami reconfigurable metasurfaces

Guobang Jiang [1,2,8], Yingying Wang[2,3,8], Ziyu Zhang[1], Weikang Pan[2,3], Yizhen Chen[2,3], Yang Wang[1], Xiangzhong Chen[4,5,6], Enming Song [4,6], Gaoshan Huang [1,4,5,6], Qiong He[2,7], Shulin Sun [2,3,5] ✉, Jizhai Cui [1,2,5,6] ✉, Lei Zhou[2,7] & Yongfeng Mei [1,4,5,6]

Dynamically controlling electromagnetic waves at will is highly desired in many applications, but most previously realized mechanically reconfigurable metasurfaces are of restricted wave-control capabilities due to the limited tuning ranges of structural properties (e.g., lattice constant or meta-atoms). Here, we present mechanically reconfigurable metasurfaces in which both lattice constants and local reflection phases of constitutional meta-atoms can be synchronously controlled based on the kirigami rotation transformation, thereby exhibiting extended tuning ranges and thus wave-control capabilities. In particular, such metasurfaces can exhibit continuously varied and even re-formed reflection-phase profiles along with the kirigami rotation transformation, serving as ideal platforms to achieve reconfigurable beam steering in pre-designed manners. Using this concept, we design and fabricate two kirigami metasurfaces, working as a beam flipper and as a beam splitter for microwaves, respectively, and experimentally characterize their wave-manipulation functionalities. Experimental results are in good agreement with full-wave simulations. The proposed idea is so general that it can be applied to realize reconfigurable metasurfaces with different materials/configurations or in high frequency regimes, for controlling electromagnetic waves and other classical waves (e.g., acoustic waves).

Metamaterials are artificial materials that possess unique mechanical[1,2], optical[3-8], electrical[9], magnetic[10], thermal[11,12] and acoustic[13-15] properties not found in nature. In general, these physical properties depend on carefully designed functional elements (known as meta-atoms) as well as their geometric arrangements[16]. Reconfigurable metamaterials possess stimuli-responsive mechanism to manipulate either the physical properties of functional meta-atoms or their spatial distribution, facilitating tunable material or physics characteristics to meet the versatile demands in practical applications[17-19]. Recently, significant efforts have been devoted to reconfigurable planar optical metasurfaces, known as the two-dimensional version of metamaterials[20-22]. Most previous works have concentrated on controlling the basic

[1]Department of Materials Science, Fudan University, Shanghai 200438, People's Republic of China. [2]Shanghai Key Laboratory of Metasurfaces for Light Manipulation, Fudan University, Shanghai 200433, People's Republic of China. [3]Shanghai Engineering Research Centre of Ultra Precision Optical Manufacturing, Department of Optical Science and Engineering, School of Information Science and Technology, Fudan University, Shanghai 200433, People's Republic of China. [4]Institute of Optoelectronics, Shanghai Frontiers Science Research Base of Intelligent Optoelectronics and Perception, Fudan University, Shanghai 200438, People's Republic of China. [5]Yiwu Research Institute of Fudan University, Yiwu 322000 Zhejiang, People's Republic of China. [6]International Institute of Intelligent Nanorobots and Nanosystems, Fudan University, Shanghai 200438, People's Republic of China. [7]State Key Laboratory of Surface Physics and Key Laboratory of Micro and Nano Photonic Structures (Ministry of Education), Fudan University, Shanghai 200433, People's Republic of China. [8]These authors contributed equally: Guobang Jiang, Yingying Wang. ✉e-mail: sls@fudan.edu.cn; jzcui@fudan.edu.cn
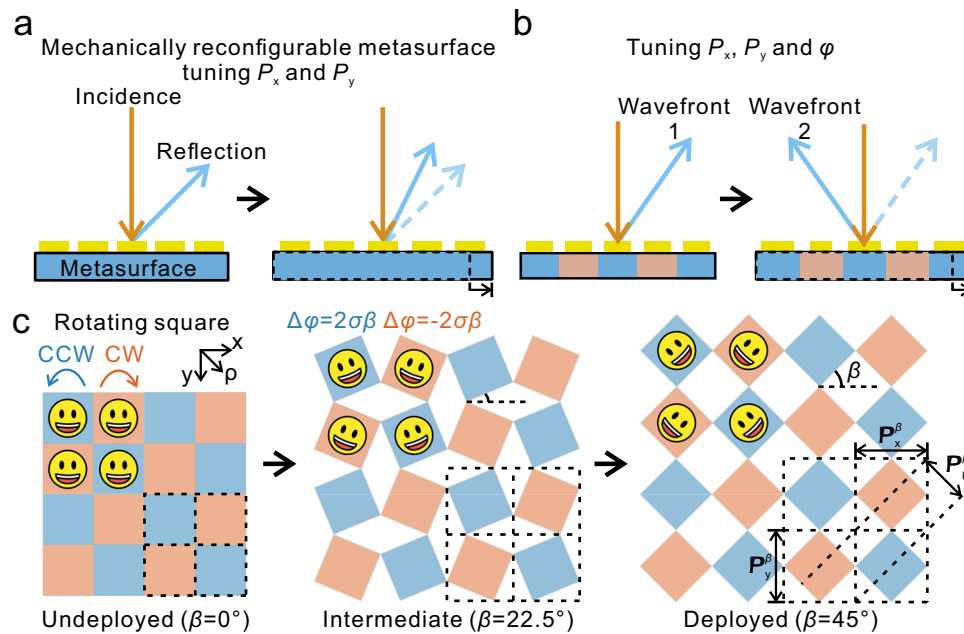
Fig. 1 | Schematic of the proposed reconfigurable kirigami metasurface.
a Conventional mechanically reconfigurable metasurfaces that adjust the angle of anomalous reflection beam by changing the lattice constants P_x and P_y through substrate deformation. **b** Proposed mechanically reconfigurable metasurfaces that can synchronously adjust the three DoFs of the meta-atoms: P_x, P_y and φ, achieving significantly extended tuning angle range of reflection beam. **c** Schematics of the adopted RS kirigami pattern composed of rigid square panel connected at the corner. During the global mechanical transformation, the blue squares rotate CCW while the red squares rotate CW. The emojis, representing arbitrary meta-atoms, rotate along with the panels. β is defined as the rotation angle of the panels, and the geometric phase variation of each meta-atom is $\Delta\varphi = \pm 2\sigma\beta$ depending on its rotation direction (CW or CCW) and polarization state of illuminated light ($\sigma = +1$: LCP; $\sigma = -1$: RCP). P_x^β, P_y^β, and P_ρ^β are the lattice constants in different transformation states along x, y and ρ direction, respectively. The emoji image is reproduced from openmoji.org under the CC BY-SA 4.0 license.

optical responses, such as the amplitude and phase, of the meta-atoms by applying electrical[23–25], thermal[26–28] or optical[29–31] stimuli to the constituent stimuli-responsive materials. As different materials are required for reconfigurable metasurfaces operating in various frequency bands[32,33], this strategy is limited to a few specific bands for the metasurfaces with particular materials. In addition, the reconfigurable metasurfaces that possess various tuning functions usually suffer from the issues of high cost, fabrication difficulty, low-efficiency and/or complex control system.

Alternatively, reconfigurable metasurfaces can be achieved by mechanically altering the spatial arrangement of meta-atoms[21] which are usually optimized to exhibit the local responses owing to the weak near-field interactions. As a result, the physical properties of meta-atoms almost remain invariant during mechanical transformation. This unique characteristic allows a purely geometric design strategy applicable to a wide range of frequency bands and material systems, as controlling spatial arrangement is independent of the scale and the constituent materials. Recently, the mechanically reconfigurable metasurfaces have led to switchable transmission characteristics[34], or wavefront shaping applications such as tunable beam deflection[35] and beam re-focusing[36]. However, substrate deformation that only changes the lateral dimension and result in the slight adjustments to lattice constants P_x and P_y (Fig. 1a), limiting the tuning range (e.g., a few degrees modulation in beam bending). While a kind of mechanical metadevices[37–39] employing motor array to individually rotate local meta-atoms enables the complex beam steering effect, they still encounter challenges such as bulky system and complex control process, and are not applicable to microscale devices. Therefore, a promising strategy for constructing mechanically reconfigurable metasurfaces that can provide both broad applicability and extensive tuning range is still crucial.

In this work, we develop a strategy that significantly extends the tuning range and functionality of mechanically reconfigurable metasurfaces by synchronously manipulating the three degrees of freedom (DoFs): phase retardation φ, lattice constants P_x and P_y, as illustrated in Fig. 1b. This allows sophisticated manipulations of electromagnetic (EM) responses, such as beam steering and reconfigurable wavefront shaping. The optical geometric phases are adjusted through mechanically rotating the orientations of the meta-atoms during the transformation of their substrates, which is carefully designed based on a "Rotating Square" (RS) kirigami pattern. When the meta-atoms are designed with a linear or a checkerboard-liked phase profile, we realize mechanically reconfigurable microwave metasurfaces as a beam flipper or a beam splitter, demonstrating the programmability of the global phase profile. Both far-field experiments and full wave simulations nicely verify the theoretical predictions. This approach for creating reconfigurable kirigami meta-devices can not only be further applied to the high frequency bands but also open up wide possibilities for research areas like magnetic and acoustic metamaterials.

Results

Synchronously tuning the three degrees of freedom by rotating square kirigami

The geometric phase (also known as Pancharatnam-Berry phase, PB phase)[40–43] can be flexibly tuned by changing the geometric orientation angle α in the kirigami metasurfaces, offering an important degree of freedom for dynamically controlling EM waves. Generally, for the reflection type meta-atom, its optical property is characterized by a Jones matrix, $J(0) = \begin{bmatrix} r_{xx} & r_{xy} \\ r_{yx} & r_{yy} \end{bmatrix}$. When the unit cell undergoes a geometric rotation of α, the Jones matrix can be re-written as: $J(\alpha) = R(\alpha)J(0)R(-\alpha)$, where $R(\alpha) = \begin{bmatrix} \cos\alpha & -\sin\alpha \\ \sin\alpha & \cos\alpha \end{bmatrix}$ is the rotation matrix. Under the illumination of left-handed circularly polarized (LCP) wave described by Jones vector $E_L = \begin{bmatrix} 1 \\ i \end{bmatrix}$, the reflected wave of the

meta-atom is described as:

$$E_{\text{refl}} = J(\alpha)E_{\text{L}} = \frac{1}{2}\left(r_{xx} + r_{yy} + ir_{xy} - ir_{yx}\right)\begin{bmatrix}1\\i\end{bmatrix}$$
$$+ \frac{1}{2}e^{i2\alpha}\left(r_{xx} - r_{yy} + ir_{xy} + ir_{yx}\right)\begin{bmatrix}1\\-i\end{bmatrix} \quad (1)$$

where $e^{i2\alpha}$ is interpreted as geometric phase carried by the cross-polarized reflection beam. Conversely, for the right-handed circularly polarized (RCP) wave (i.e., $E_{\text{R}} = \begin{bmatrix}1\\-i\end{bmatrix}$) illumination, the meta-atom with the same orientation α will obtain the geometric phase $e^{-i2\alpha}$ for its cross-polarized reflection beam. Therefore, the obtained phase shift φ of each meta-atom is related to its geometric orientation α with the relation $\varphi = \sigma 2\alpha$, where $\sigma = \pm 1$ represent the LCP and RCP illumination, respectively.

We propose the strategy of combining the orientation-dependent PB phase and the kirigami technique to construct the reconfigurable metasurfaces. Origami and kirigami are the East Asian art of paper folding and cutting, and have attracted significant research interest in the field of metasurfaces due to their programmable transformations through the operations of creases and cuts of design patterns[44–49]. In particular, the RS kirigami pattern exhibits auxetic properties (possessing negative Poisson's ratio) and thus emerges as a powerful transformation mechanism for mechanically reconfigurable metasurfaces, which allows synchronous elongation or contraction in both lateral directions[50]. Additionally, each square unit in the RS pattern can continuously rotate during the transformation, enabling the flexible controls over the physics properties of the device.

Figure 1c depicts the characteristics of the RS kirigami transformation. The RS pattern is a tessellation of squares, with kirigami cuts along the edge that allow for panel rotation relative to the hinges at the corners. During the transformation, each red and blue panel rotates clockwise (CW) or counter-clockwise (CCW), respectively. We define the initial state as the undeployed state with $\beta = 0°$ (Fig. 1c, left panel). Here, β is the intersection angle between the bottom edges of the square panels and x axis. In the deployed states with $\beta = 22.5°$ and $\beta = 45°$, the RS kirigami is partially and fully expanded, respectively (Fig. 1c, middle and right panels).

During the transformation, the meta-atoms (illustrated by the emojis in Fig. 1c) rotate along with the square panels at the same angle, which will result in a change of the orientation relating to the panel rotation β, i.e., $\Delta\alpha = \pm\beta$ (+: CCW rotation; -: CW rotation). Considering the nature of geometric phase, the change of geometric phase Δφ of meta-atoms on each panel is $\Delta\varphi = 2\sigma\beta$ for the meta-atoms on the blue panels and $\Delta\varphi = -2\sigma\beta$ for the meta-atoms on the red panels, in which σ represents the chirality of the incident circularly polarized (CP) waves. This mechanism provides an artful manipulation of the phase difference between neighboring meta-atoms. Moreover, the lattice constants, including both P_x and P_y, can be effectively adjusted due to the auxetic behavior of RS pattern, as depicted in Fig. 1c. Clearly, P_x always equals P_y during the transformation, which satisfy the relation to the panel rotation angle β as:

$$P_x^\beta = P_y^\beta = \sqrt{2}P_x^0 \sin\left(\beta + \frac{\pi}{4}\right) \quad (2)$$

Therefore, all these DoFs (phase φ and lattice constants P_x^β, P_y^β) can be flexibly controlled by the panel rotation angle β of the RS kirigami pattern, providing a powerful technique for dynamic manipulations.

Phase distribution design for anomalous reflection
We next introduce the proposed kirigami reconfigurable metasurfaces for achieving exotic beam bending effect. Theoretically, the

generalized Snell's law of reflection[3,51] describes the correlation between the phase gradient and anomalous reflection of the metasurface:

$$\sin\theta_r - \sin\theta_i = \frac{\lambda}{2\pi n_i}\frac{d\varphi}{d\rho} \quad (3)$$

where θ_i is the incident angle, θ_r is the reflection angle, λ represents the wavelength of the incident beam, n_i is the refractive index of the incident medium (mostly air), and $\frac{d\varphi}{d\rho}$ represents the phase gradient introduced by the metasurface along the pre-defined direction.

To achieve high-performance wavefront controls, we adopt optimization technique to design a PB meta-atom, which is composed of an A-shaped metallic microstructure and a metallic mirror separated by a dielectric spacer ($\varepsilon_r = 2.6$), as shown in Fig. 2a. Some detailed parameters are listed here: $a = 6\,\text{mm}$, $w = 0.4\,\text{mm}$, $b = 2.1\,\text{mm}$, $h = 1.5\,\text{mm}$ and $\xi = 90°$. Such unit cell in metal-insulator-metal (MIM) configuration can totally reflect the incident waves and thus block all transmission channels.

We next evaluate the polarization conversion ratio (PCR) of the proposed meta-atoms, which will determine the efficiency of the geometric phase based meta-devices. According to Eq. (1), it is noted that only the second term $e^{i2\alpha}(r_{xx} - r_{yy} + ir_{xy} + ir_{yx})$ (i.e., the polarization conversion term) exhibits a geometric phase and contributes to the wavefront controls for the composite gradient PB metasurface, e.g., anomalous reflection. Meanwhile, the first co-polarization term, representing the normal reflection, should be eliminated. Supposing that the meta-atoms satisfy the mirror symmetry, the off-diagonal terms in the reflection Jones matrix equals to zero, i.e., $r_{xy} = r_{yx} = 0$. Therefore, designing a high efficiency PB meta-atom should satisfy the criterion $r_{xx} + r_{yy} = 0$. For a lossless reflection geometry, the reflection amplitudes $|r_{xx}|$ and $|r_{yy}|$ remains at 100% in the concerned frequency range. Therefore, the desired meta-atoms need to satisfy $\varphi_{yy} - \varphi_{xx} = \pi$, implying an effective half wave plate capable of completely switching the polarization of the incident CP wave[43,52]. Figure 2b shows the simulated and measured spectra of reflection amplitudes $|r_{xx}|$, $|r_{yy}|$ and reflection phase $\varphi_{xx}, \varphi_{yy}$ of a periodic array of the A-shaped meta-atoms (See Methods), exhibiting a phase difference of about π in a broad frequency band. Based on these data, the PCR defined as the efficiency of the anomalous reflection mode carrying cross polarization (i.e., $|(r_{xx} - r_{yy})/2|^2$) can be straightly retrieved as shown in Fig. 2c. It is clear that the designed meta-atom achieves a high PCR (> 0.8) across a frequency range of 12.5 – 16 GHz, fulfilling the desired criterion quite well.

Rotating square kirigami metasurface as a beam flipper
We first design a reconfigurable kirigami metasurface as a beam flipper, which can not only control but also flip the anomalous reflection beam. Such metasurface in the undeployed state ($\beta = 0°$) satisfy the linear geometric phase distribution. We can see that the orientation of adjacent meta-atoms has a constant difference of 45° along both x and y direction, the angular bisector of whose intersection angle is defined the ρ direction, corresponding to the geometric phase difference of 90°, as shown in Fig. 3a. To clearly illustrate the EM response, the color is coated on the meta-atoms representing the coded geometric phase profile. In the undeployed state, the phase gradient is uniform and along the diagonal direction of the metasurface, resulting in a corresponding anomalous reflection beam towards the same direction. Based on Eq. (3), the reflection angle is calculated as $\theta_r^0 = 33.5°$ for the anomalous reflection beam carrying RCP at 16 GHz. During the kirigami transformation, the metasurface goes through the intermediate state ($\beta = 22.5°$, see Fig. 3b) and then to the deployed state ($\beta = 45°$, see Fig. 3c). Interestingly, the uniform phase gradient of the deployed state
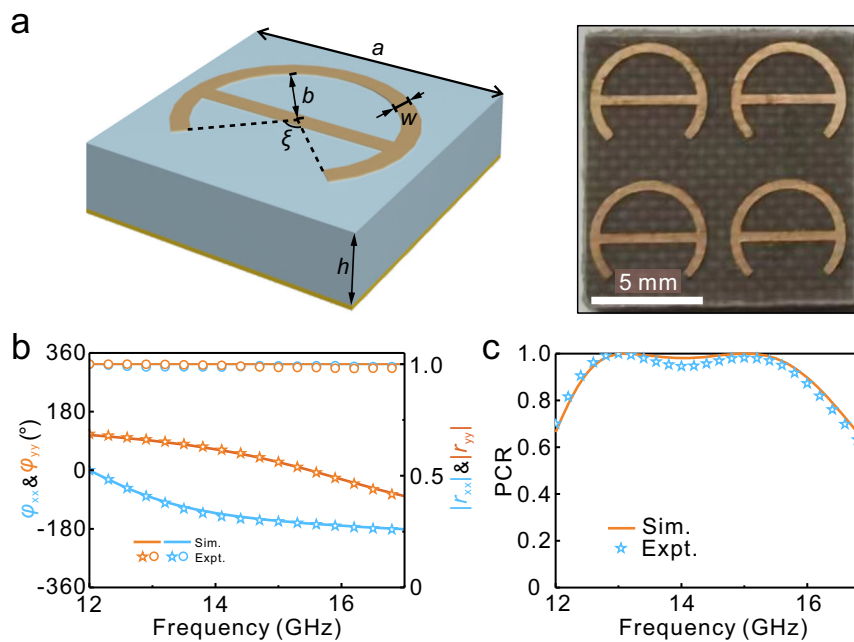
Fig. 2 | Design of a high efficiency A-shaped meta-atom. a Left: the structural parameters of the A-shaped meta-atom. Here, a, b, w, h and ξ are respectively 6 mm, 2.1 mm, 0.4 mm, 1.5 mm and 90°. Right: top view photograph of a rigid panel consisting of 2×2 meta-atoms. Scale bar, 5 mm. **b** Experimentally measured and FDTD-simulated reflection amplitudes $|r_{xx}|$, $|r_{yy}|$ and reflection phase φ_{xx}, φ_{yy} of the meta-atom array when normally illuminated by x-polarized and y-polarized EM waves, respectively. **c** PCR of the meta-atoms retrieved from the measurement and simulation data. Source data are provided as a Source Data file.

is reversed in comparison with that of the undeployed state, resulting in a flipped anomalous reflection beam along $\theta_r^{\frac{\pi}{2}} = -23°$. In the intermediate state the phase profile turns to a binary pattern with a 180° difference, therefore resulting in the symmetric anomalous dual-beams generations along $\theta_r^{\frac{\pi}{4}} = \pm25°$. Meanwhile, the normal reflection mode is completely blocked by the destructive interference effect. It should be noted that the lattice constants also increase as the kirigami metasurface transform from $\beta = 0°$ to 45°, enabling the continuously tuned reflection angle.

Following the aforementioned design, we fabricate a transformable kirigami resin substrate with 3D-printer and attach them with the pre-designed meta-atoms fabricated through common PCB technique (see Methods and Supplementary Fig. S1). The meta-atoms are then assembled with the desired spatially varied phase profile to form the reconfigurable PB metasurface. The transformation process and the three representative states, i.e., undeployed, intermediate and deployed states of the metasurface are shown in Supplementary Movie S1 and Fig. 3d–f, respectively. The color coated on the top microstructures illustrates the phase information of the metasurface in the corresponding transformation states. We perform far-field angular scanning measurement to detect the normalized electric field intensity of the reflected EM waves (see Methods) in the diagonal plane defined by the phase gradient. Here, the metasurface is illuminated by the normally incident linear polarized (LP) EM waves at 12-17 GHz, and is detected by an RCP antenna to obtain the angular distributions of the scattering field as shown in Fig. 3g–i. We can find that the reflection angles of the deflected beam in the undeployed, intermediate and deployed states are approximately +33.5°, ±25° and −23°, respectively, agreeing well with the theoretical predictions. The finite-difference time-domain (FDTD) simulation results are presented in Supplementary Fig. S2, showing good agreement with the experimental ones. Due to the polarization-correlated nature of PB device, the scattered fields carrying LCP will propagate along the symmetric directions, as shown in Supplementary Fig. S3.

Indeed, the proposed reconfigurable kirigami metasurface can achieve the broadband beam tuning and flipping. Figure 3g(ii), h(ii)

and i(ii) illustrate the measured scattered field intensity as function of the working frequency and reflection angle. At the broad frequency band from about 12.5 to 16.5 GHz, the anomalous reflection mode dominates within entire reflection angle region, which is consistent with the theoretical prediction. Meanwhile, outside this frequency window, the metasurface reflects most incident light along the specular direction, attributing to the relatively low PCR at these frequencies.

We next provide a comprehensive analysis on the functionality of the kirigami metasurface during the full RS transformation process from $\beta = 0°$ to 90° (see Supplementary Fig. S4). As β increases from 45° to 90°, the metasurface exhibits the totally same phase gradient to the cases of β varying from 45° to 0°. For example, we provide the experimental and simulated results of the anomalous reflection effect for the kirigami substrate at $\beta = 67.5°$ and $\beta = 90°$ (Supplementary Fig. S5), which demonstrate the identical functionalities to that at $\beta = 22.5°$ (Fig. 3h) and $\beta = 0°$ (Fig. 3g), respectively. Relying on the three tunable DoFs, the tuning range of the beam flipper can cover the range of $(-33.5°, -23°] \cup (23°, 33.5°]$ in the whole transformation process.

Further, we examine the coupling efficiency of all reflection modes as well as transmission modes of the kirigami metasurface as β increase from 0° to 45°, as shown in Supplementary Fig. S6. The measured efficiencies of anomalous reflection mode are 97.5%, 50.7% and 36.5% in the undeployed state, intermediate state and deployed state, respectively, which fit well with the simulation results. Here, the efficiency is defined as the ratio between the energy carried by the desired mode to that carried by the input waves, which are obtained through integrating the measured/calculated energy over the corresponding angular region. Considering that the air gaps between adjacent meta-atoms become larger in the transformation process, we notice that the efficiency of normal transmission mode increases from 0 to about 52%. Since meta-atoms designed in reflection configuration will not induce the phase retardation for the transmission beam, the anomalous transmission mode will thus not exist as demonstrated by the results shown in Supplementary Fig. S6. On the other hand, the anomalous reflection mode will gradually become weak, with its efficiency decreasing from nearly
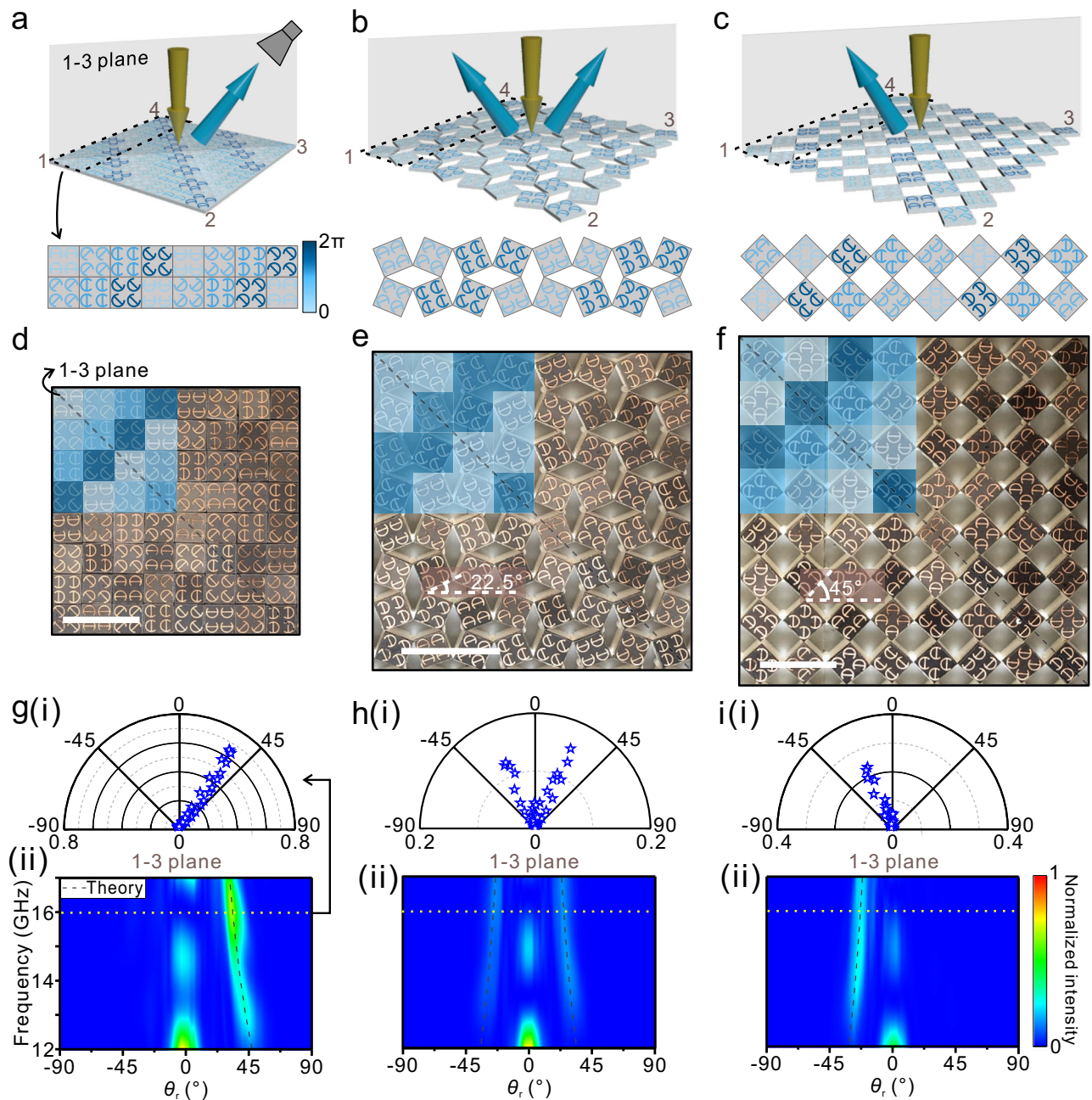
Fig. 3 | Experimental demonstration of the reconfigurable metasurface as a beam flipper. a–c Schematics of the beam flipper exhibiting different beam bending effect in 1-3 plane in undeployed ($\beta = 0°$), intermediate ($\beta = 22.5°$) and deployed states ($\beta = 45°$), respectively. Here, the geometric phase profiles carried by the devices for LCP illumination case are denoted by the color mapped on the meta-atoms, which satisfy the linear, binary and inversely linear distributions along r direction in the three states. The yellow and blue arrows represent the incident LP beam and the anomalous reflection CP beam, respectively. **d–f** Optical photographs of the fabricated beam flipper in the three states. Color mapped on each photograph indicates the encoded geometric phase distribution for the devices. Scale bar, 30 mm. **g–i (i)** Experimentally measured electric field intensity

distributions of reflection beam with RCP at 16 GHz and **(ii)** within the frequency range of 12–17 GHz for the metasurface in three states. The field intensities at different angles are normalized against a reference signal, which is the received electric field intensity at $\theta_r = 0°$ when the same incident beam is reflected by a flat metal with the same size of the metasurface sample. Here, the dashed line represents the theoretical prediction of the anomalous reflection angle. These results demonstrate the reconfigurable beam bending effects, including the single-beam anomalous reflection, dual-beam anomalous reflection as well as flipped single-beam anomalous reflection, based on the RS kirigami transformation. Source data are provided as a Source Data file.

100% to 42%. In the whole transformation process, the intensity of normal reflection mode almost remains zero, justifying the robust high-performance of the metasurfaces.

Rotating square kirigami metasurface as a beam splitter

We also design another kirigami metasurface by setting the initial geometric phase difference between adjacent meta-atoms, exhibiting

the reconfigurable functionalities between four anomalous beams splitting and single normal mode reflection during the transformation, as shown in Fig. 4a–c. In the undeployed state ($\beta = 0°$), the metasurface are composed of two different super cells (consisting of 4×4 identical meta-atoms) with the orientation difference of 90°, displaying a checkerboard-liked phase profile with the phase difference of 180° between adjacent pixels, as shown in Fig. 4a. Such device, behaving like
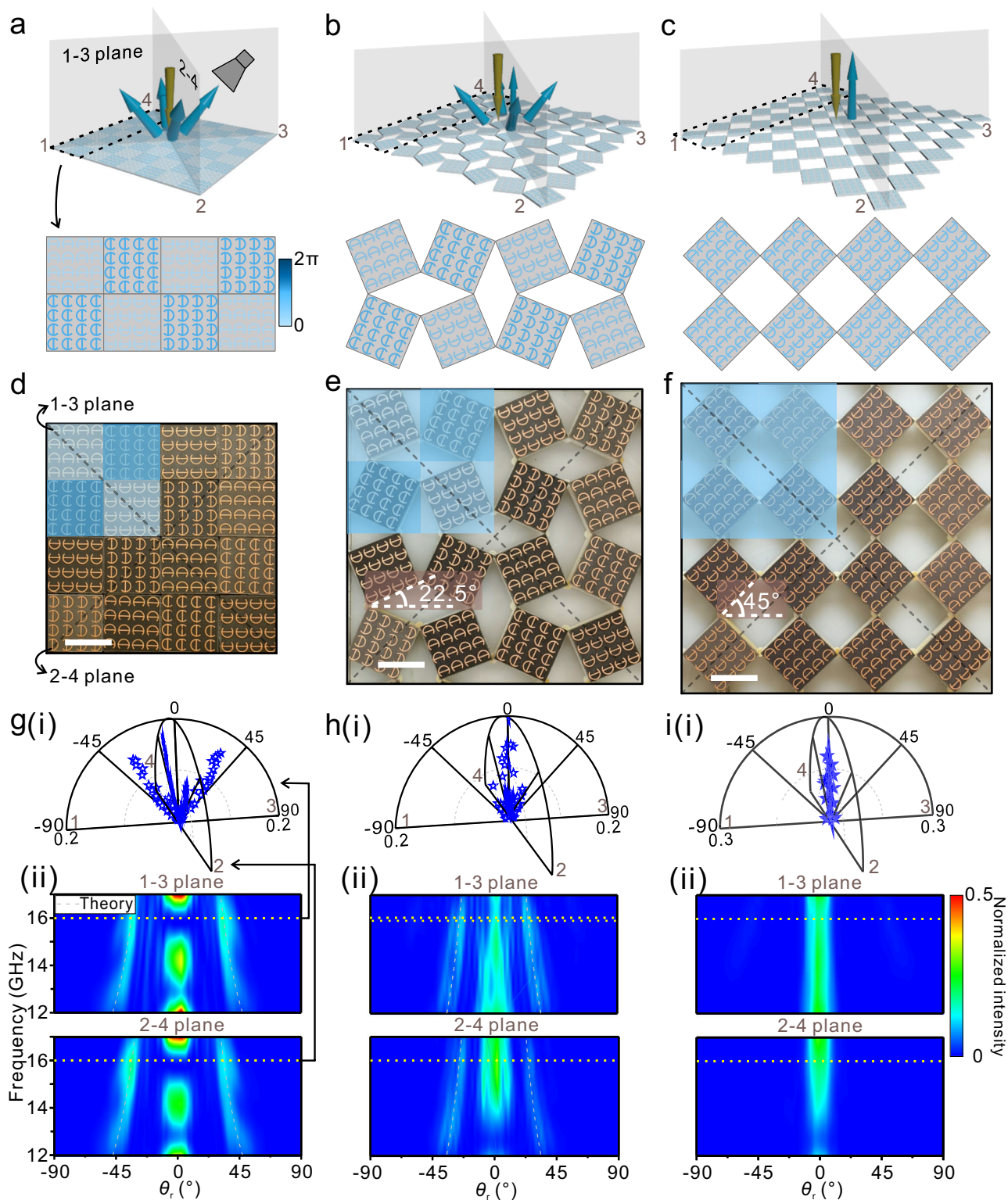
Fig. 4 | Experimental demonstration of the reconfigurable metasurface as a beam splitter. a–c Schematics of the beam splitter exhibiting reconfigurable beam reflecting effect at 1–3 and 2–4 plane in undeployed ($\beta = 0°$), intermediate ($\beta = 22.5°$) and deployed states ($\beta = 45°$), respectively. Here, the geometric phase profiles carried by the devices for LCP illumination case are denoted by the color mapped on the meta-atoms, which satisfy the checkerboard-liked, sub-checkerboard and uniform distributions in the three states. The yellow and blue arrows represent the incident LP beam and the anomalous reflection CP beam, respectively. **d–f** Optical photographs of the fabricated beam splitter in the three states. Colors mapped on each

photograph indicates the encoded geometric phase distributions for the device. Scale bar, 20 mm. **g–i** (i) Experimentally measured electric field intensity distributions of reflection beam with RCP at 16 GHz and (ii) within the frequency range of 12-17 GHz for the beam splitter in the three states. The field intensities at different angles are normalized against a reference signal, similar to the beam flipper. Here, the dashed line represents the theoretical prediction of the anomalous reflection angle. These results demonstrate the reconfigurable beam controlling effects, i.e., a switching between four split reflection beams and a specular reflection beam based on the RS kirigami transformation. Source data are provided as a Source Data file.

two-dimensional grating, will divide the incident LP light to four different anomalous reflection modes carrying the equal intensities. The anomalous reflection angle defined by the intersection angle between the reflected beam and z-axis is $\theta_r^0 = 33.5°$ at 16 GHz according to the grating equation. Interestingly, in the deployed state (i.e., $\beta = 45°$) as shown in Fig. 4c, since all meta-atoms exhibit the same phase, the whole device behave like a flat mirror with periodic air holes. As a result, the four anomalous reflection modes originating from diffraction effect are suppressed and the single normal reflection mode thus dominates. In the intermediate state (i.e., $\beta = 22.5°$) as shown in Fig. 4b, although the phase profile also exhibits the binary behavior, the phase difference of two super cells changes to 90°. Therefore, the normal reflection mode cannot be completely terminated, resulting in the co-existing behavior of both the normal specular reflection mode and anomalous reflection modes.

We adopt far-field scanning measurements to verify the fabricated metasurface for beam splitting, with its transformation process shown in Supplementary Movie S1. In the experiments, we illuminate the metasurface with a LP normally incident EM wave of 12–17 GHz and utilize an RCP antenna to collect the angular distributions of the scattering far-field intensity. Figure 4g–i shows the experimentally measured normalized reflection beam intensity distributions at 16 GHz of the metasurface in the undeployed state, intermediate state, deployed state, respectively. Since the anomalous reflection modes propagates along the two diagonal planes (denoted as 1–3 and 2–4 planes as depicted in Fig. 4) of the device, the far-field scanning measurements are performed at these two perpendicular planes, respectively. In the undeployed state (Fig. 4g(i)), the four beams are clearly observed, with a measured reflection angle about 33.5°. In the intermediate state (Fig. 4h(i)), the intensity of the four split beams is notably reduced while the normal reflection mode emerges simultaneously. Owing to the scaling of the lattice constant, the anomalous reflection angle changes to about 25°. In the whole transformation process ($\beta = 0°$-45°), the reflection angle of the anomalous beam can be tuned within the range of $(23°, 33.5°]$. In the deployed state (Fig. 4i(i)), only normal specular reflection mode remains. The broadband response of the proposed reconfigurable metasurface is also demonstrated by the experiments, as shown in Fig. 4g(ii)–i(ii). It should be noted that the LCP components of the reflection beams exhibit the same reflection behaviors, which will not be discussed in the main-text. FDTD simulation results of the metasurfaces in different states are presented in Supplementary Figs. S7 and S8. All of the experimental and simulated results nicely agree with the theoretical analysis.

We also analyze the phase profiles and the functionalities for the kirigami metasurface in the state from $\beta = 0°$ to $\beta = 90°$ as shown in Supplementary Figs. S9 and S10. It is clear that the present device shows the same functionalities between the regions of $\beta \in [0°, 45°]$ and $\beta \in [45°, 90°]$. The anomalous (or normal) reflection efficiencies of the splitter in the undeployed, intermediate and deployed state are respectively 95.6% (or 4.4%), 32.6% (or 22.7%), and 4.0% (or 37%). The experimental results fit well with the simulation results (see Supplementary Fig. S10). Except for the desired anomalous reflection modes illustrated in Figs. 3 and 4, the other diffraction modes are quite weak and therefore not discussed in the main text (see more details in Supplementary Fig. S11).

Discussion

In summary, we developed a strategy for the design of mechanical metasurfaces that can synchronously modulate all three DoFs of the meta-atoms (i.e., phase φ and lattice constants P_x and P_y) based on the RS kirigami transformation, resulting in the reconfigurable EM wavefront engineering. As a proof-of-concept, we design and fabricate two kirigami metasurfaces, including a beam flipper and a beam splitter, that are not achievable with current mechanically reconfigurable

metasurfaces. Moreover, we also propose an RS-based metalens (see Supplementary Fig. S12) to demonstrate the generality of the proposed kirigami design concept for reconfigurable wavefront controls. The transformation of the proposed kirigami metasurface inevitably introduces air gaps, resulting in the undesired transmission mode and the reduced efficiency of anomalous reflection. To address this issue, we explore a potential solution by designing the cascaded metasurfaces that can compensate for the air-gap-induced transmission loss (see numerical demonstration in Supplementary Note 1). Indeed, this strategy paves up a broad future direction for dynamic metadevices. Extensive researches on mechanical metamaterials has already identified numerous RS-derived kirigami patterns[53], which allow for customizable anisotropic rotations of the meta-atoms. It is noted that, although the correlation of three degrees of freedom is hard to break through such transformation process, many different kirigami patterns—such as rotating rectangles or triangles—could also offer a broad design space for us. Additionally, creating super cells by placing different meta-atoms on a single rotational panel can further expand the design space for advanced optical functionalities. Furthermore, with advancements in micro- and nano-fabrication techniques[54,55], microscale kirigami devices have been recently realized with carefully designed cuts and creases connecting adjacent rigid panels[56–58], allowing the size of such kirigami-based reconfigurable metasurfaces to be conveniently scaled down, and thus making them suitable for applications in higher frequencies.

It is also worth noting that orientation-dependent physical properties have been investigated in various metamaterials. For example, magnetic coupling strength strongly depends on the orientation of magnetic dipoles[10]. In electronics, meta-atoms covered with carefully designed, separate circuits enable metamaterial to vary their output signals through simple rotations[9]. Recent work on acoustic metamaterials has demonstrated phase change of acoustic waves by the geometric rotation of cascaded metagratings[59]. Therefore, we believe the strategy proposed in this paper, which utilizes kirigami rotation transform of the meta-atoms to actively modulate the overall physical response of metamaterials, has the potential to achieve more complex functionalities across multiple research fields.

Methods

Fabrication of Kirigami metasurface

The kirigami metasurface are fabricated by combining the EM responsive meta-atoms and the 3D printed transformable substrate. The meta-atoms are fabricated based on a copper coated 1.5mm-thick dielectric FR4 board ($\varepsilon_r = 2.6$), on which the top layer is the copper A-shaped resonator and the bottom layer is a continuous copper film. The transformable substrate is the 3D printed resin with the same side length of the meta-atoms. The 2×2 or 4×4 identical meta-atoms are utilized as super cells of two devices and then fixed on the equally sized transformable substrate with spatially varied orientations, eventually forming the kirigami patterned metasurfaces.

Simulation and measurement of devices

In both numerical simulations and experimental measurements of beam flipping and splitting effects, the PB metasurfaces are illuminated by linearly polarized EM waves, which can be decomposed into a superposition of LCP and RCP components[60]. To obtain the measurement results in Figs. 3 and 4, an RCP antenna is used as the receiver to detect the reflection signals. The normal and anomalous reflection modes collected by the same RCP antenna, originating from the LCP and RCP components of input beams, will propagate along specular and non-specular directions, respectively. Therefore, using the same RCP detector allows us to collect both the normal and anomalous reflection modes in a single measurement process. To obtain the reference signal, the metasurface is replaced by a metal plate of the same size to measure the specular reflection signal using the RCP antenna as the receiver and the

LP antenna as the source. After integrating the energy of the anomalous (or normal) reflection beam over the non-specular (specular) angle regime, we can obtain its conversion efficiency which is defined as the integrated energy divided by the reference value (i.e., half of the energy of the input LP beam). If utilizing the CP antenna as the source, we need to employ respectively RCP and LCP horn antennas as the receivers to perform the measurements, considering that the normal mode and anomalous mode will carry different CP states. Obviously, the number of measurements required would double in this case. Considering that all PB devices exhibit co-related functionalities for two different CP states, we only present the experimental results of the RCP reflection mode in the main text, whereas the results for the LCP component are shown in Supplementary Information. For comparison, all simulation results for the proposed metasurfaces are also presented in Supplementary Information.

In practical measurements, an LP horn antenna and a CP horn antenna are connected to a network analyzer (Agilent E8362C PNA) as transmitter and receiver, respectively. The LP horn antenna is positioned vertically aligned with the center of the sample to illuminate a normally incident wave. Both horn antennas are placed at 1.8 m away from the sample, and the CP horn antenna is rotated on a circular track to detect the scattered far-field intensity at the different reflection angles. After the kirigami metasurfaces are transformed to the certain states, some local meta-atoms deviating from the desired rotation angles are adjusted to ensure the uniformity. The metasurfaces are then attached to a highly transparent acrylic board to improve their stability. In both experiments and simulations, the electric field intensities at different angles are normalized against a reference signal, which is the received electric field intensity at $\theta_r = 0°$ when the same incident beam is reflected by a flat metal with the same size of the metasurface.

Additionally, the LP source and receiver are employed for both numerical simulations and experimental measurements. By aligning the polarization directions of two LP antennas parallel to the x-axis (or y-axis) of the meta-atoms, we can obtain the reflection amplitude $|r_{xx}|$ (or $|r_{yy}|$) and phase φ_{xx} (or φ_{yy}). Here, the reflection coefficients are normalized to the reference signals obtained by performing the same measurement on a same-sized metallic plate.

Data availability
All the data supporting the findings of this study are provided in the Supporting Information and Source Data file. Source data are provided with this paper.

References

1. Zheng, X. et al. Ultralight, ultrastiff mechanical metamaterials. *Science* **344**, 1373 (2014).
2. Bertoldi, K., Vitelli, V., Christensen, J. & van Hecke, M. Flexible mechanical metamaterials. *Nat. Rev. Mater.* **2**, 17066 (2017).
3. Yu, N. et al. Light propagation with phase discontinuities: generalized laws of reflection and refraction. *Science* **334**, 333 (2011).
4. Liu, N. et al. Three-dimensional photonic metamaterials at optical frequencies. *Nat. Mater.* **7**, 31 (2008).
5. Wang, S. et al. Broadband achromatic optical metasurface devices. *Nat. Commun.* **8**, 187 (2017).
6. Pu, M. et al. Catenary optics for achromatic generation of perfect optical angular momentum. *Sci. Adv.* **1**, e1500396 (2015).
7. Deng, Z. L. et al. Diatomic metasurface for vectorial holography. *Nano Lett.* **18**, 2885 (2018).
8. Pors, A., Nielsen, M. G., Eriksen, R. L. & Bozhevolnyi, S. I. Broadband focusing flat mirrors based on plasmonic gradient metasurfaces. *Nano Lett.* **13**, 829 (2013).
9. El Helou, C., Grossmann, B., Tabor, C. E., Buskohl, P. R. & Harne, R. L. Mechanical integrated circuit materials. *Nature* **608**, 699 (2022).
10. Louis, D. et al. A tunable magnetic metamaterial based on the dipolar four-state Potts model. *Nat. Mater.* **17**, 1076 (2018).
11. Liu, X. et al. Taming the blackbody with infrared metamaterials as selective thermal emitters. *Phys. Rev. Lett.* **107**, 045901 (2011).
12. Jin, P. et al. Deep Learning-Assisted Active Metamaterials with Heat-Enhanced Thermal Transport. *Adv. Mater.* **36**, 2305791 (2023).
13. Cummer, S. A., Christensen, J. & Alù, A. Controlling sound with acoustic metamaterials. *Nat. Rev. Mater.* **1**, 16001 (2016).
14. Ma, G. & Sheng, P. Acoustic metamaterials: From local resonances to broad horizons. *Sci. Adv.* **2**, e1501595 (2016).
15. Zhang, X. & Liu, Z. Extremal transmission and beating effect of acoustic waves in two-dimensional sonic crystals. *Phys. Rev. Lett.* **101**, 264303 (2008).
16. Yu, N. & Capasso, F. Flat optics with designer metasurfaces. *Nat. Mater.* **13**, 139 (2014).
17. Sun, S., He, Q., Hao, J., Xiao, S. & Zhou, L. Electromagnetic metasurfaces: physics and applications. *Adv. Opt. Photon* **11**, 380 (2019).
18. Kim, J. et al. Dynamic Hyperspectral Holography Enabled by Inverse-Designed Metasurfaces with Oblique Helicoidal Cholesterics. *Adv. Mater.* **36**, 2311785 (2024).
19. Cui, T. J., Qi, M. Q., Wan, X., Zhao, J. & Cheng, Q. Coding metamaterials, digital metamaterials and programmable metamaterials. *Light Sci. Appl.* **3**, e218 (2014).
20. Zheludev, N. I. & Kivshar, Y. S. From metamaterials to metadevices. *Nat. Mater.* **11**, 917 (2012).
21. He, Q., Sun, S. & Zhou, L. Tunable/Reconfigurable Metasurfaces: Physics and Applications. *Res. (Wash. D. C.)* **2019**, 1849272 (2019).
22. Pettine, J. et al. Light-driven nanoscale vectorial currents. *Nature* **626**, 984 (2024).
23. Li, L. et al. Electromagnetic reprogrammable coding-metasurface holograms. *Nat. Commun.* **8**, 197 (2017).
24. Zhang, L. et al. Space-time-coding digital metasurfaces. *Nat. Commun.* **9**, 4334 (2018).
25. King, J. et al. Electrically tunable VO2–metal metasurface for mid-infrared switching, limiting and nonlinear isolation. *Nat. Photon* **18**, 74 (2023).
26. Kats, M. A. et al. Ultra-thin perfect absorber employing a tunable phase change material. *Appl Phys. Lett.* **101**, 221101 (2012).
27. Chen, B. et al. Directional terahertz holography with thermally active Janus metasurface. *Light Sci. Appl* **12**, 136 (2023).
28. Zhang, S. et al. Thermal tuning nanoprinting based on liquid crystal tunable dual-layered metasurfaces for optical information encryption. *Opt. Express* **32**, 4639 (2024).
29. Wang, Q. et al. Optically reconfigurable metasurfaces and photonic devices based on phase change materials. *Nat. Photon* **10**, 60 (2015).
30. Qu, G. et al. Reprogrammable meta-hologram for optical encryption. *Nat. Commun.* **11**, 5484 (2020).
31. Wang, H. et al. All-optical ultrafast polarization switching with nonlinear plasmonic metasurfaces. *Sci. Adv.* **30**, eadk3882 (2024).
32. Pan, M. et al. Dielectric metalens for miniaturized imaging systems: progress and challenges. *Light Sci. Appl* **11**, 195 (2022).
33. Naik, G. V., Shalaev, V. M. & Boltasseva, A. Alternative plasmonic materials: beyond gold and silver. *Adv. Mater.* **25**, 3264 (2013).
34. Yang, Y., Vallecchi, A., Shamonina, E., Stevens, C. J. & You, Z. A new class of transformable kirigami metamaterials for reconfigurable electromagnetic systems. *Sci. Rep.* **13**, 1219 (2023).
35. Zhuang, X. et al. Active terahertz beam steering based on mechanical deformation of liquid crystal elastomer metasurface. *Light Sci. Appl* **12**, 14 (2023).
36. Zheng, Y. et al. Kirigami reconfigurable gradient metasurface. *Adv. Funct. Mater.* **32**, 2107699 (2021).
37. Yang, W. et al. Angular-adaptive reconfigurable spin-locked metasurface retroreflector. *Adv. Sci. (Weinh.)* **8**, e2100885 (2021).
38. Xu, Q. et al. Mechanically reprogrammable Pancharatnam–Berry metasurface for microwaves. *Adv. Photon* **4**, 016002 (2022).
39. Fan, Z. et al. Homeostatic neuro-metasurfaces for dynamic wireless channel management. *Sci. Adv.* **8**, eabn7905 (2022).

40. Bomzon, Z. E., Biener, G., Kleiner, V. & Hasman, E. Space-variant Pancharatnam–Berry phase optical elements with computer-generated subwavelength gratings. *Opt. Lett.* **27**, 1141 (2002).
41. Huang, L. et al. Dispersionless phase discontinuities for controlling light propagation. *Nano Lett.* **12**, 5750 (2012).
42. Ding, X. et al. Ultrathin pancharatnam-berry metasurface with maximal cross-polarization efficiency. *Adv. Mater.* **27**, 1195 (2015).
43. Luo, W., Xiao, S., He, Q., Sun, S. & Zhou, L. Photonic spin hall effect with nearly 100% efficiency. *Adv. Opt. Mater.* **3**, 1102 (2015).
44. Schenk, M. & Guest, S. D. Geometry of Miura-folded metamaterials. *Proc. Natl Acad. Sci. USA* **110**, 3276 (2013).
45. Rafsanjani, A. & Bertoldi, K. Buckling-Induced Kirigami. *Phys. Rev. Lett.* **118**, 084301 (2017).
46. Choi, G. P. T., Dudte, L. H. & Mahadevan, L. Programming shape using kirigami tessellations. *Nat. Mater.* **18**, 999 (2019).
47. Shen, Y. et al. Origami-inspired metamaterial absorbers for improving the larger-incident angle absorption. *J. Phys. D. Appl. Phys.* **48**, 445008 (2015).
48. Xu, L. et al. Kirigami nanocomposites as wide-angle diffraction gratings. *ACS Nano* **10**, 6156 (2016).
49. Wang, Z. et al. Origami-based reconfigurable metamaterials for tunable chirality. *Adv. Mater.* **29**, 1700412 (2017).
50. Grima, J. N. & Evans, K. E. Auxetic behavior from rotating squares. *J. Mater. Sci. Lett.* **19**, 1563 (2000).
51. Sun, S. et al. Gradient-index meta-surfaces as a bridge linking propagating waves and surface waves. *Nat. Mater.* **11**, 426 (2012).
52. Pan, W. et al. High-efficiency generation of far-field spin-polarized wavefronts via designer surface wave metasurfaces. *Nanophotonics* **11**, 2025 (2022).
53. Liu, L., Choi, G. P. T. & Mahadevan, L. Wallpaper group kirigami. *Proc. R. Soc. A* **477**, 20210161 (2021).
54. Shyu, T. C. et al. A kirigami approach to engineering elasticity in nanocomposites through patterned defects. *Nat. Mater.* **14**, 785 (2015).
55. Hong, X. et al. Optoelectronically navigated nano-kirigami micro-rotors. *Sci. Adv.* **10**, eadn7582 (2024).
56. Cui, J. et al. Nanomagnetic encoding of shape-morphing micro-machines. *Nature* **575**, 164 (2019).
57. Liu, Q. et al. Electronically configurable microscopic meta-sheet robots. *Nat. Mater.* https://doi.org/10.1038/s41563-024-02007-7 (2024).
58. Smart, C. et al. Magnetically programmed diffractive robotics. *Science* **386**, 1031 (2024).
59. Liu, B. et al. Experimental verification of the acoustic geometric phase. *Appl. Phys. Lett.* **120**, 211702 (2022).
60. Dong, S. et al. Broadband spin-unlocked metasurfaces for bifunctional wavefront manipulations. *Appl. Phys. Lett.* **120**, 181702 (2022).

Acknowledgements

Author contributions

J.C., G.J. and S.S. conceived the project and wrote the manuscript. G.J. fabricated the sample. G.J. and Y.Y.W. conducted the numerical simulations and performed the measurement. W.P., Q.H. and S.S. provided useful suggestions on experiments and simulations. Y.Y.W., L.Z., and Y.M. co-wrote the manuscript. Z.Z., Y.C., Y.W., X.C., E.S., G.H., and Q.H. discussed the results and commented on the manuscript.

Competing interests

The authors declare no competing interests.

Additional information

Supplementary information The online version contains supplementary material available at https://doi.org/10.1038/s41467-025-56211-3.

Correspondence and requests for materials should be addressed to Shulin Sun or Jizhai Cui.

Peer review information *Nature Communications* thanks the anonymous reviewer(s) for their contribution to the peer review of this work. A peer review file is available.

Reprints and permissions information is available at http://www.nature.com/reprints

Publisher's note Springer Nature remains neutral with regard to jurisdictional claims in published maps and institutional affiliations.